Journal of Fluorescence (2025) 35:2347–2363
https://doi.org/10.1007/s10895-024-03688-8

RESEARCH

Synthesis and Photophysical Characterizations of Benzimidazole Functionalized BODIPY Dyes

Gökhan Sevinç[1] · Emine Doğan[1] · Sina Mansuroğlu[2] · Rafig Gurbanov[2,3]

Received: 10 February 2024 / Accepted: 22 March 2024 / Published online: 8 April 2024

Abstract

Herein, a series of new BODIPY dyes substituted by 2-phenyl benzimidazole units at the *meso* (C8) position including methyl/ethyl, phenyl, or *p*-methoxyphenyl moieties at the distal and proximal positions of the BODIPY core have been successfully synthesized and their photophysical characteristics were analyzed. Experimentally investigating absorption and fluorescence profiles in the THF media was followed by density functional theory (DFT) calculations to clarify photophysical features. Theoretical analyses have revealed that upon excitation, both electrons and holes are confined solely within the BODIPY core. The energy levels of the frontier molecular orbitals converge depending on the presence of the phenyl and *p*-methoxyphenyl substituents. The orbital distributions of both electron and hole were in the -3 and -5 positions, which demonstrates a continuous conjugation with the BODIPY core at these sites. However, the electron density present on the phenyl rings located at the -1, -7, and -8 (*meso*) positions was found to be negligible. The benzimidazole-BODIPYs exhibited photodynamic activity (Φ_Δ) ranging from ~ 7% to ~ 11%, determined by a comparative method. Moreover, the compounds have shown to maintain their stability thermally in a non-reactive/inert environment up to temperatures surpassing 300 °C, exhibiting primarily a two-phase decomposition process. These compounds have the potential to function as antibacterial and anti-biofilm agents when used in concentrations ranging from 0.5 to 2.0 mg/mL. The results provide a basis for evaluating heterocyclic benzimidazole units on photophysical processes containing BODIPY chromophores.

Keywords Benzimidazole · Benzimidazole-BODIPY · Fluorescence · DFT

Introduction

The design and synthesis of fluorescent dyes for practical applications is an essential research topic. Among the organic-based molecules, 4,4-difluoro-4-bora-3a,4a-diaza-*s*-indacene compounds, namely BODIPYs (Fig. 1a-b), have been investigated in diverse topics such as dye-sensitized solar cells DSSCs [1–3], non-linear optical materials [4–6], bioimaging agents [7, 8] and especially chemical sensors [9–11]. Indeed, the burgeoning interest in BODIPY research is largely attributed to their unique photophysical attributes, coupled with the vast array of functionalization options that enable precise adjustments to their optoelectronic characteristics within the visible spectrum. These heterocyclic molecules have been the subject of increasing amounts of research over the years due to their high absorption coefficients, elevated photostability, narrow fluorescence bandwidths, high fluorescence quantum yields, and openness to chemical modifications [12–17]. Therefore, extensive efforts have been devoted to the synthesis of the BODIPY-based dyes to determine the photophysical parameters.

The aromatic aldehyde and pyrrole derivatives are widely used as starting materials in the one-pot synthesis procedures of the BODIPY skeletons [18, 19]. BODIPYs are amenable to several types of reactions, which allow the introduction of different kinds of substituents on the BODIPY core for fine-tuning the electronic properties of the chromophore. Following the synthesis of the main structure, the required

✉ Gökhan Sevinç
gokhan.sevinc@bilecik.edu.tr

✉ Rafig Gurbanov
rafig.gurbanov@bilecik.edu.tr

[1] Faculty of Science, Department of Chemistry, Bilecik Seyh Edebali University, TR 11100 Bilecik, Turkey

[2] Department of Bioengineering, Bilecik Seyh Edebali University, Engineering Faculty, TR 11100 Bilecik, Turkey

[3] Central Research Laboratory (BARUM), Bilecik Seyh Edebali University, 11100 Bilecik, Turkey

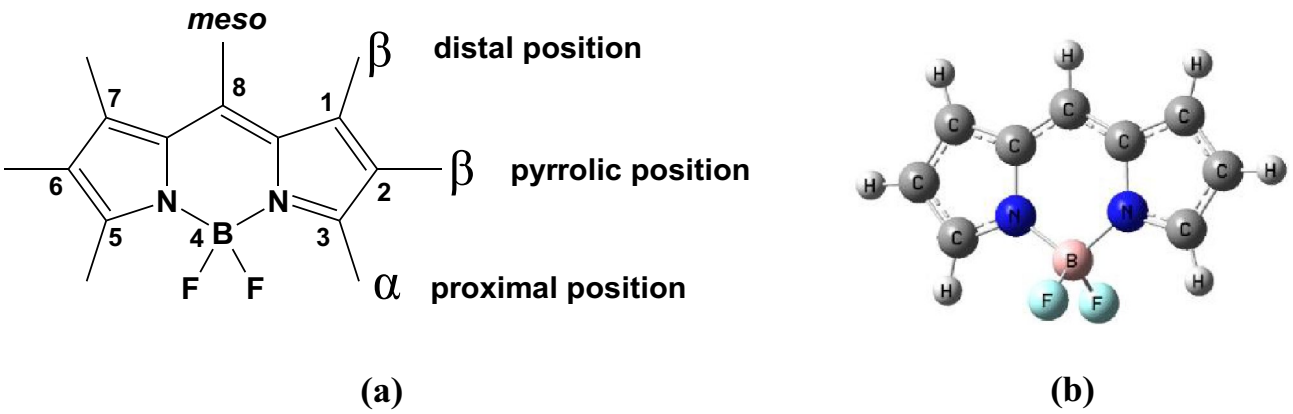

Fig. 1 **a** Borondipyrromethene (BODIPY) core and positions on it. **b** planar geometry of the BODIPY structure calculated by the Density functional theory (DFT) in gas phase

atoms or groups can be included in the BODIPYs can be further modified by introducing necessary atoms or groups. Common reactions employed for this purpose include halogenation [20], sulfonation [21], Knoevenagel condensation [22], Suzuki–Miyaura coupling, [23] and Sonogashira [24] reactions are common. However, one of the less explored functionalization pathways is the post-functionalization via formyl groups at the meso (8) position of the BODIPY core. In this regard, the functionalization of BODIPYs via the formyl group may enable the preparation of complex compounds with different molecular structures, such as BODIPY-heterocyclic conjugates.

BODIPY-heterocyclic conjugates have shown to alter the photophysical parameters of the BODIPY core due to donor–acceptor interactions between the heterocyclic matrix and the chromophore. As a heterocyclic structure, benzimidazole is a fused aromatic imidazole ring system (Fig. 2) where a benzene ring is fused to the 4 and 5 positions of an imidazole ring. Benzimidazole is also named 3-azaindole and some derivatives have been subjected to diverse photophysical and biological research [25–28].

There have been some studies on BODIPY-benzimidazole conjugates, primarily focusing on their photophysical and bioimaging properties, in recent years [29–31, 6, 32–35]. To our knowledge, the photophysical properties of BODIPYs, which have phenyl groups in both the distal and proximal positions on the BODIPY core and the benzimidazole ring in the *meso* (8) position, have not been studied. Hence, the integration of the arylated BODIPY core and benzimidazole structures on one molecule via the aldehyde group is expected to produce new fluorescent materials that have absorption and fluorescence features over a wide range of the visible region spectra due to extended conjugation and/or donor–acceptor interactions.

In the present work, the BODIPYs containing phenyl, *p*-methoxyphenyl, and methyl/ethyl groups at distal and proximal positions of the BODIPY core, as well as heterocyclic benzimidazole structures on the *meso* (8) position were systematically designed and synthesized using formyl substituted BODIPYs as precursors. The study also investigated how the attachment of benzimidazole groups and aryl units to the conjugates influences their photophysical characteristics, including photodynamic activities. To clarify the photophysical properties, theoretical calculations were performed using density functional theory (DFT) and time-dependent density functional theory (TD-DFT) approaches. By performing electron–hole analyses, the charge transfer cases between the connected structures and the substituted aryl/alkyl groups were examined and the experimental photophysical properties were successfully elucidated. The chemical structures were characterized using ^{1}H NMR, FTIR, and HRMS techniques. Since the thermal stability of synthetic compounds affects their use and applications in various analytical systems, thermal profiles were characterized by thermogravimetric analysis (TGA).

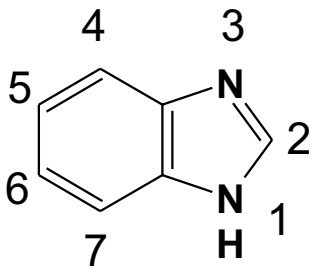

Fig. 2 Numbering system in benzimidazole cycle

Experimental Section

Materials and Instruments

The compounds were synthesized using the reagents obtained from Merck without further purification. Solvents used for spectroscopy measurements were spectroscopic grade and were purchased from Merck. The reactions were monitored using TLC-aluminum sheets with silica gel (Merck 60 F_{254}) and a UV lamp. Column chromatography was performed using silica gel 60 (230—400 mesh). HRMS spectra were recorded on Agilent 6224 LC/MS High Resolution Mass Time-of-Flight (HRMS) spectrometer in positive or negative mode. Perkin–Elmer 100 spectrometer (equipped with ATR unit) was used for FT-IR spectra of the compounds in the range 650–4000 cm^{-1}. ^{1}H-NMR spectra were obtained with a Bruker Avance 500 MHz spectrometer in $CDCl_3$ with TMS as an internal standard while ^{13}C NMR spectra were recorded at 125 MHz in the same solvent. Chemical shifts (δ) were given in ppm relative to solvent peaks ($CDCl_3$: ^{1}H: δ 7.26; ^{13}C: δ 77.4). The coupling constants (*J*) were reported in hertz. Thermogravimetric analysis (TGA) of the final BODIPYs was performed by heating the compounds with Exstar SII TGA/DTA 7200 device under nitrogen flow with a heating rate of 10 °C / min in the range of 20–1100 °C. The synthesis of the starting aldehyde 4-(5,5-dimethyl-1,3-dioxan-2-yl)benzaldehyde [36], compounds **A1**, **A2, A3** [36]**,** and 2,4-diphenyl1-*H* pyrrole derivatives were achieved according to our reported procedures [37, 38].

Synthesis

2,4-Dimethyl-3-ethyl-8-[4-(4,4-Dimethyl-2,6-dioxan-1-yl) benzaldehyde]-4,4′-difluoroboradiazaindacene (A1)

4-(5,5-dimethyl-1,3-dioxan-2-yl)benzaldehyde (1.00 g, 4.54 mmol) and 2,4-dimethyl-3-ethylpyrrole (1.35 mL, 9.98 mmol) was dissolved in dry dichloromethane (150 mL) and the solution was purged with N_2 through for 5 min. To this solution, 1 drop of trifluoroacetic acid (TFA) was added and stirred at room temperature for 24 h. The color changed slowly from pale brown to red. Depletion of the aldehyde was observed by TLC. The oxidizing agent *p*-Chloranil (1.67 g, 6.81 mmol) was added and the mixture was stirred for 24 h at room temperature. N,N-diisopropylethylamine (5.30 mL) was then added, followed by a subsequent addition of BF_3.OEt_2 (6.30 mL) dropwise. The mixture was stirred for another 24 h at room temperature. The reaction was terminated and neutralized by the addition of saturated aqueous $NaHCO_3$ (100 mL), and was then washed 2 times with pure water. The organic layer was dried over Na_2SO_4, filtered and the solvent evaporated. Chromatography on silica gel ($CHCl_3$) gave the compound **A1** as an orange-red powder. Yield: 538 mg (24%). FTIR (ATR, cm^{-1}) ν_{max}: 2965, 1536, 1474, 1393, 1314, 1272, 1188, 1158, 1099, 1077, 1020, 975, 835, 761, 711, 662. ^{1}H-NMR (500 MHz, $CDCl_3$): δ[ppm]: 0.86 (s, 3H), 0.99 (t, *J*:7.5 Hz, 6H), 1.29 (s, 6H), 1.36 (s, 3H), 2.31 (q, J_1: 7.5 Hz, J_2: 7.5 Hz, 4H), 2.56 (s, 6H), 3.72 (d, *J*:11.0 Hz, 2H), 3.85 (d, *J*:11.5 Hz, 2H), 5.49 (s, 1H), 7.33 (d, *J*:8.5 Hz, 2H), 7.65 (d, *J*:8.0 Hz, 2H). HRMS (Q-TOF-ESI) (m/z) Calcd: 494.29162 ($C_{29}H_{37}BF_2N_2O_2$), found: 494.29214 $[M]^+$, Δ = 1.05 ppm.

4, 4-difluoro-8-[4-(4,4-Dimethyl-2,6-dioxan-1-yl) benzaldehyde]-1,3,5,7-tetraphenyl-4-bora-3a,4a-diaza-*s*-indacene (B1)

4-(5,5-dimethyl-1,3-dioxan-2-yl)benzaldehyde (1.00 g, 4.54 mmol) and 2,4-diphenyl-*1H*-pyrrole (2.09 g, 9.53 mmol) was dissolved in dry dichloromethane (150 mL) and N_2 was purged for 5 min. To this solution, 1 drop of trifluoroacetic acid (TFA) was added, followed immediately by *p*-Chloranil (1.57 g, 6.40 mmol). The reaction mixture was stirred at room temperature for 24 h. The reaction mixture was then concentrated about 30 mL on a rotary evaporator and filtered through a filter paper. The green-colored filtrate was washed with water and extracted with $CHCl_3$ (3 × 30 mL). The solvent was evaporated, resulting solid was dried and solved in DCM (100 mL). N,N-diisopropylethylamine (4.95 mL), and BF_3.OEt_2 (5.95 mL) were added respectively. The mixture was stirred for 24 h at room temperature. The reaction was stopped and neutralized by the addition of saturated aqueous $NaHCO_3$ (100 mL), and was then washed 2 times with pure water. The organic layer was dried over Na_2SO_4, filtered and the solvent evaporated. Column chromatography on silica gel (elution: $CHCl_3$) gave the compound **B1** as a red powder. Yield: 1.53 g (49%). FTIR (ATR, cm^{-1}) ν_{max}: 2923, 2866, 2842, 1536, 1514, 1494, 1472, 1452, 1400, 1363, 1301, 1225, 1168, 1136, 1111, 1047, 1032, 825, 761, 696, 662. ^{1}H-NMR (500 MHz, $CDCl_3$): δ[ppm]: 0.83 (s, 3H), 1.24 (s, 3H), 3.56 (d, *J*:10.5 Hz, 2H), 3.70 (d, *J*:11.0 Hz, 2H), 5.03 (s, 1H), 6.55 (s, 2H), 6.59 (d, *J*:8.0 Hz, 2H), 6.74 (d, *J*:7.0 Hz, 4H), 6.84 (d, *J*:8.0 Hz, 2H), 6.87 (t, *J*:7.5 Hz, 4H), 6.91 (d, *J*:7.5 Hz, 2H), 7.45 (d, *J*:7.5 Hz, 6H), 7.91 (d, *J*:6.5 Hz, 4H). HRMS (Q-TOF-ESI) (m/z) Calcd: 686.29162 ($C_{45}H_{37}BF_2N_2O_2$), found: 687.29688 $[M+H]^+$, Δ = 3.74 ppm.

4,4-difluoro-8-[4-(4,4-Dimethyl-2,6-dioxan-1-yl)benzaldehyde]-1,3,5,7-[4-methoxyphenyl]-4-bora-3a,4a-diaza-s-indacene (C1)

C1 was synthesized using the method described above. 4-(5,5-dimethyl-1,3-dioxan-2-yl)benzaldehyde (1.00 g, 4.54 mmol), 2,4-bis(4-methoxyphenyl)-*1H*-pyrrole (2.66 g, 9.53 mmol), *p*-Chloranil (1.57 g, 6.40 mmol), N,N-diisopropylethylamine (4.95 mL) and $BF_3.OEt_2$ (5.95 mL) were used in the reaction. The crude product was chromatographed (elution: $CHCl_3$) to afford 1.43 g (yield: 39%) of **C1** as a red powder. FTIR (ATR, cm^{-1}) ν_{max}: 2943, 2866, 2844, 1607, 1491, 1469, 1432, 1388, 1235, 1146, 1099, 1052, 1032, 1017, 943, 887, 822, 775, 726, 652. ^{1}H-NMR (500 MHz, $CDCl_3$): δ[ppm]: 0.81 (s, 3H), 1.26 (s, 3H), 3.56 (d, *J*:10.5 Hz, 2H), 3.70–3.65 (m, 8H), 3.88 (s, 6H), 5.02 (s, 1H), 6.40 (d, *J*:8.5 Hz, 4H), 6.50 (s, 2H), 6.65 (d, *J*:8.5 Hz, 6H), 6.83 (d, *J*:8.0 Hz, 2H), 6.98 (d, *J*:9.0 Hz, 4H), 7.91 (d, *J*:9.0 Hz, 4H). HRMS (Q-TOF-ESI) (m/z) Calcd: 806.33391 ($C_{49}H_{45}BF_2N_2O_6$), found: 806.34126 $[M]^+$, Δ = 5.11 ppm.

General Procedure for the Preparations of Formyl-BODIPYs A2, B2 and C2

Compound **A1** (300 mg, 0.61 mmol) and trifluoroacetic acid (3.0 mL) in 9:1, CH_2Cl_2:H_2O (20 mL, v/v) solution was stirred at room temperature for 6 h. The organic layer was then washed with water, dried with Na_2SO_4, and evaporated to dryness. The crude product was chromatographed (elution: $CHCl_3$) to afford 150 mg (yield: 60%) of **A2** as a red powder. FTIR (ATR, cm^{-1}) ν_{max}: 2968, 2926, 2871, 1701, 1607, 1536, 1474, 1390, 1319, 1269, 1183, 1077, 1054, 975, 835, 800, 758, 706, 662. ^{1}H-NMR (500 MHz, $CDCl_3$): δ[ppm]: 1.00 (t, *J*: 8.0 Hz, 6H), 1.28 (s, 6H), 2.32 (q, J_1: 7.5 Hz, J_2: 7.5 Hz, 4H), 2.56 (s, 6H), 7.53 (d, *J*: 8.5 Hz, 2H), 8.04 (d, *J*: 8.0 Hz, 2H), 10.15 (s, 1H). HRMS (Q-TOF-ESI) (m/z) Calcd: 408.21846 ($C_{24}H_{27}BF_2N_2O$), found: 408.21902 $[M]^+$, Δ = 1.37 ppm.

B2 as a red powder was obtained using the synthetic method described above. (268 mg, 60% yield). FTIR (ATR, cm^{-1}) ν_{max}: 2923, 2847, 1701, 1536, 1514, 1491, 1469, 1452, 1396, 1358, 1300, 1272, 1225, 1143, 1111, 1032, 946, 832, 756, 694, 662. ^{1}H-NMR (500 MHz, $CDCl_3$): δ[ppm]: 6.56 (s, 2H), 6.75 (d, *J*: 7.0 Hz, 4H), 6.83 (t, *J*: 7.0 Hz, 4H), 6.90 (t, *J*: 7.0 Hz, 2H), 7.00 (d, *J*: 8.0 Hz, 2H), 7.05 (d, *J*: 8.0 Hz, 2H), 7.47 (d, *J*: 7.5 Hz, 6H), 7.92 (d, *J*: 8.0 Hz, 4H), 9.66 (s, 1H). HRMS (Q-TOF-ESI) (m/z) Calcd: 600.21846 ($C_{40}H_{27}BF_2N_2O$), found: 581.22199 $[M-F]^+$, Δ = 3.32 ppm.

C2 was obtained as a red powder using the synthetic method described above. (270 mg, 62% yield). FTIR (ATR, cm^{-1}) ν_{max}: 2971, 2936, 2837, 1696, 1607, 1570, 1551, 1501, 1469, 1432, 1390, 1274, 1249, 1232, 1185, 1136, 1104, 1072, 1030, 941, 889, 830, 773, 716. ^{1}H-NMR (500 MHz, $CDCl_3$): δ[ppm]: 3.61 (s, 6H), 3.89 (s, 6H), 6.36 (d, *J*: 9.0 Hz, 4H), 6.51 (s, 2H), 6.66 (d, *J*: 8.5 Hz, 4H), 7.00 (d, *J*: 9.0 Hz, 4H), 7.03 (d, *J*: 8.0 Hz, 2H), 7.09 (d, *J*: 8.0 Hz, 2H), 7.92 (d, *J*: 9.0 Hz, 4H), 9.71 (s, 1H). HRMS (Q-TOF-ESI) (m/z) Calcd: 720.26073 ($C_{44}H_{35}BF_2N_2O_5$), found: 720.25599 $[M]^+$, Δ = 2.02 ppm.

General Procedure for the Preparations of Benzimidazole-BODIPYs A3, B3, B4 and C3

Compound **A2** (110 mg, 0.27 mmol) and o-phenylenediamine (36 mg, 0.33 mmol) were dissolved in 10 mL DMF. Then, *p*-TsOH (2.4 mg, 0.014 mmol) was added and the solution was heated and stirred at 80 °C for 5 h. The mixture was cooled to room temperature and poured into 1 M Na_2CO_3 solution (50 mL). The Precipitate was filtered and washed with water, dried and the crude product was chromatographed (elution: $CHCl_3$) to afford 69 mg (yield: 51%) of **A3** as a red solid. FTIR (ATR, cm^{-1}) ν_{max}: 2953, 2928, 2864, 1546, 1474, 1449, 1427, 1321, 1190, 1161, 1119, 1074, 980, 847, 763, 741, 719, 696. ^{1}H-NMR (500 MHz, $CDCl_3$): δ[ppm]: 0.98 (t, *J*: 15.0 Hz, 6H), 1.32 (s, 6H), 2.30 (q, J_1: 7.5 Hz, J_2: 7.5 Hz, 4H), 2.57 (s, 6H), 7.34–7.32 (m, 2H), 7.46 (d, *J*: 8.5 Hz, 2H), 7.72 (s, 2H), 8.30 (d, *J*: 8.0 Hz, 2H). ^{13}C-NMR (125 MHz, $CDCl_3$) δ: 154.3, 154.2, 150.3, 138.7, 138. 2, 138.1, 133.2, 130.5, 129.4, 127.6, 127.4, 126.3, 123.8, 17.1, 14.6, 12.6, 12.0. HRMS (Q-TOF-ESI) (m/z) Calcd: 496.26099 ($C_{30}H_{31}BF_2N_4$), found: 497.26846 $[M+H]^+$, Δ = 0.70 ppm.

B3 was obtained as a red solid using the synthetic method described above. Yield: 102 mg, 55%. FTIR (ATR, cm^{-1}) ν_{max}: 3395, 2926, 1533, 1514, 1494, 1469, 1449, 1422, 1393, 1361, 1269, 1225, 1141, 1069, 1047, 1032, 1020, 948, 837, 790, 761, 743, 694, 664. ^{1}H-NMR (500 MHz, $CDCl_3$): δ[ppm]: 6.56 (s, 2H), 6.78 (d, *J*: 8.0 Hz, 4H), 6.81 (d, *J*: 7.5 Hz, 2H), 6.84 (d, *J*: 7.0 Hz, 4H), 7.03 (d, *J*: 8.0 Hz, 2H), 7.45–7.44 (m, 6H), 7.38–7.36 (m, 2H), 7.91–7.90 (m, 4H), 7.75 (s, 2H), 6.93–6.89 (m, 2H). ^{13}C-NMR (125 MHz, $CDCl_3$) δ: 157.6, 147.8, 143.9, 137.6, 135.8, 135.2, 132.9, 132.6, 132.4, 132.2, 129.7, 129.5, 128.9, 128.8, 128.2, 127.7, 127.5, 127.3, 126.7, 126.6, 123.6. HRMS (Q-TOF-ESI) (m/z) Calcd: 688.26099 ($C_{46}H_{31}BF_2N_4$), found: 687.25525 $[M-H]^-$, Δ = 3.04 ppm.

By using 4-Chloro-*o*-phenylenediamine, the same procedure was followed for the synthesis of **B4** as a red solid (80 mg, 40% yield). FTIR (ATR, cm^{-1}) ν_{max}: 3385, 2923, 1538, 1514, 1496, 1469, 1452, 1417, 1361, 1299, 1225, 1143, 1050, 1032, 946, 924, 840, 788, 763, 696, 662. ^{1}H-NMR (500 MHz, $CDCl_3$): δ[ppm]: 6.58 (s, 2H), 6.83–6.76 (m, 12H), 7.00 (d, *J*: 7.5 Hz, 2H), 7.46–7.44 (m, 8H), 7.92–7.90 (m, 5H). ^{13}C-NMR (125 MHz, $CDCl_3$) δ: 154.3, 151.4, 142.9, 136.3, 136.0, 135.3, 132.5, 130.6, 130.1, 129.5, 129.1, 128.8, 128.2, 127.9, 127.7, 127.3, 126.9,

126.7, 126.0, 123.3, 122.9, 119.8. HRMS (Q-TOF-ESI) (m/z) Calcd: 722.22201 ($C_{46}H_{30}BClF_2N_4$), found: 721.21704 $[M-H]^-$, Δ = 3.95 ppm.

Compound **C3** as a red solid was obtained by following the procedure in the synthesis of **A3**. Yield: 75 mg, 34%. FTIR (ATR, cm^{-1}) v_{max}: 2938, 2844, 1607, 1546, 1489, 1472, 1435, 1390, 1249, 1178, 1141, 1106, 1032, 948, 889, 825, 743, 654. ^{1}H-NMR (500 MHz, $CDCl_3$): δ[ppm]: 3.31 (s, 6H), 3.84 (s, 6H), 6.35 (d, *J*: 7.0 Hz, 4H), 6.42 (d, *J*: 8.0 Hz, 1H), 6.52 (s, 2H), 6.64 (d, *J*: 6.5 Hz, 4H), 6.75 (d, *J*: 8.0 Hz, 1H), 6.99–6.94 (m, 8H), 7.35 (s, 2H), 7.92 (d, *J*: 6.5 Hz, 4H). ^{13}C-NMR (125 MHz, $CDCl_3$) δ: 160.9, 158.4, 156.9, 151.5, 147.1, 138.2, 132.8, 131.2, 130.5, 130.0, 129.1, 128.9, 127.7, 126.9, 126.0, 125.0, 123.3, 119.8, 115.1, 113.8, 113.0, 56.0, 55.2. HRMS (Q-TOF-ESI) (m/z) Calcd: 808.30327 ($C_{50}H_{39}BF_2N_4O_4$), found: 809.31691 $[M+H]^+$, Δ = 4.06 ppm.

Photophysical Measurements

The tetrahydrofuran (THF) solvent to be used in the preparation of dye solutions and for spectroscopic measurements was first taken into a flask and N_2 was passed through it for 10 min. For the preparation of solutions, concentrated stock solutions of compounds were first prepared in chloroform at a concentration of 1.0×10^{-3} M. Then, certain volumes of solutions were taken from the stock solution, chloroform was removed by evaporator, and the final solutions (2.0×10^{-6} M) were prepared by adding THF. All solutions were kept in the dark and at room temperature. The steady state UV–vis spectra of the compounds were recorded on a Shimadzu UV-1800 scanning spectrophotometer. Fluorescence spectra of the compounds were measured on a Perkin Elmer LS55 spectrophotometer. The measurements were taken within 8 h after the solution preparation. In fluorescence measurements, the excitation (input) and emission (output) slit intervals were set to 10.0 nm and 8.0 nm, respectively. A 1 cm quartz cells were used to perform general absorption and fluorescence measurements at 25 °C. Baseline corrected UV–vis spectra were collected between 200 and 1100 nm while fluorescence spectra were collected between 200–900 nm. The BODIPY dyes were excited at maximum absorption wavelengths obtained from their UV–vis spectra. The fluorescence quantum (Φ_F) yields were calculated according to the following formula (Eq. 1) using the Fluorescein reference ($\Phi_F = 0.79$ in ethanol).

$$\Phi_F = \Phi_F(\mathrm{Std})\frac{\mathrm{F.A_{Std}}.n^2}{F_{Std}.A.n^2_{Std}} \quad (1)$$

In the equation; Φ_F: quantum efficiency of the sample, Φ_F (Std): quantum yield of the reference, F: area under the fluorescence emission curves of the sample, F_{Std}: area under the fluorescence emission curves of the standard, A_{Std}: absorbance value of the standard at the excitation wavelength, A: absorbance value of the sample at the excitation wavelength, n: refractive index of the solvent used in solving and n_{Std}: refractive index of the solvent used in solving the standard.

Computational Studies

The ground state geometry optimizations of the designed BODIPYs and the excited state calculations were performed within the frameworks of DFT and time-dependent DFT (TDDFT) approaches due to their good results in the literature [38–42]. All calculations and visualizations of the title compounds **A3**, **B3**, **B4,** and **C3** were carried out with Gaussian 09 Rev. C.01 [43] and GaussView 5.0.9 [44], respectively. The B3LYP exchange–correlation functional was chosen together with 6-311G basis set for structural optimization using the Conductor-like Polarizable Continuum (CPCM) model in THF. Frequency analysis were performed after geometry optimizations to make sure that the optimized structures were true energy minima. Time-dependent DFT (TDDFT) was employed to calculate the excited state properties of the dyes by using the same functional and basis set that was used for the ground state calculations. To increase configuration coefficients accuracy in TDDFT calculations, the *IOp(9/40=4)* keyword was used. Natural transition orbitals (NTOs) were obtained from the transition density matrices calculated by TDDFT using the Multiwfn [45]. Hole-electron analysis of the final compounds was performed with the same software based on the first excited state energies from the TDDFT calculations. The density of states (DOS) diagrams was plotted using Gauss-Sum 3.0 [46].

Biological Studies

Two commonly established methods, an antibacterial activity assay, and a biofilm formation assay, were conducted as described in the literature [47–49]. Further details on the experimental methods are provided in the supplementary material.

Results and Discussion

Synthesis and Characterization

The benzimidazole substituted BODIPYs (**A3**, **B3**, **B4,** and **C3**) were synthesized over a sequence of steps as shown in Scheme 1. The procedures for the preparation are well established in the literature [36–38, 50, 51], which are performed under mild conditions with modest synthesis yields. Firstly, initial BODIPYs (**A1**, **B1,** and **C1**) were synthesized from the 2,4-diaryl pyrrole derivatives and the aromatic aldehyde-containing protecting group. Subsequently the formyl groups were formed by hydrolysis of protecting groups with

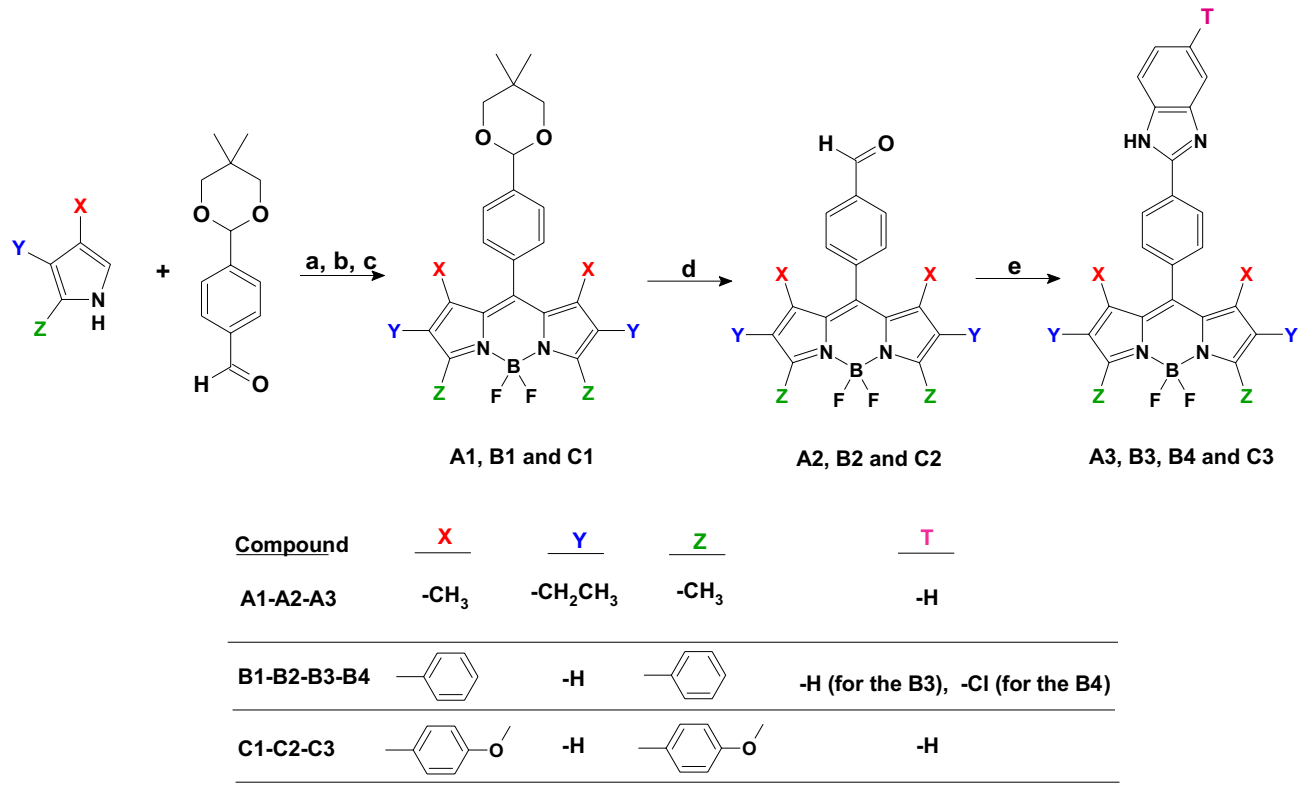

Scheme 1 The synthesis of the target molecules; **a**: dichloromethane (DCM), *catalyst.* trifluoroacetic acid; **b:** tetrachloro-*p*-benzoquinone (*p*-Chloranil), 24 h, rt; **c**: N,N-Diisopropylethylamine (Hunig's base), $BF_3.OEt_2$, 24 h, rt; **d**: CH_2Cl_2:H_2O, TFA, 6 h, rt; **e:** *o*-phenylenediamine (for the compounds **A3**, **B3** and **C3**) and 4-chloro-*o*-phenylenediamine (for the compound **B4**), N,N-Dimethylformamide (DMF), *p*-Toluenesulfonic acid (*p*-TsOH), 5 h, 80 °C

trifluoroacetic acid in DCM:H_2O media to give the compounds **A2**, **B2** and **C2**, respectively. Aldehyde groups were used as building blocks to form the benzimidazole cycle at the *meso position* (8) of the BODIPY core. In the last step, BODIPY compounds containing formyl groups were reacted with *o*-phenylenediamine derivatives in DMF under *p*-toluenesulfonic acid catalysis, and final products (**A3**, **B3**, **B4,** and **C3**) were obtained. The TLC analysis revealed the presence of new single spots for desired compounds and the disappearance of starting formyl BODIPYs.

Hence, the products were easily purified by column chromatography as they were less drifted on the silica gel in chloroform elution. The overall synthesis yields of the final products were in the order of **B3** > **B4** > **A3** > **C3**. Electron-releasing methoxy groups at the indacene rings reduced the reaction yields. Since the acid-catalyzed condensation reactions take place at the *meso* positions of the BODIPYs, the methoxyphenyl groups at the -1/-7 positions may have created a steric hindrance. On the other hand, the phenyl groups at the -1, -3, -5, and -7 positions of the indacene core are more resistant to acidic environments and temperature factors because of their lower chemical reactivity compared to the alkyl groups. Since the chemical reactivity of the methyl protons at the alpha (- α) positions of the pyrrole derivatives, increased by-product formation could be attributed to lower synthetic yields [37, 50, 52, 53]. Accordingly, yields for the aryl-decorated BODIPYs increased noticeably. For example, compound **A1** was synthesized with a yield of 24%, while **B1** and **C1** were obtained with a yield of 49% and 39%, respectively. The increasing trend is also valid for the second-stage hydrolysis reactions. In the last step, the use of chlorine-substituted *o*-phenylenediamine and methoxy groups relatively decreased the yields of acid catalyzed condensation reactions. The benzimidazole BODIPY structures were confirmed by ^{1}H NMR, ^{13}C NMR, FTIR, and HRMS techniques, ensuring that the observed data aligned precisely with the expected structures. The ^{1}H NMR measurements of the resulting compounds gave well-resolved spectra in the typical range of 0–11 ppm. Due to the intense aromatic groups in the compounds, phenyl protons appeared as multiplets in the 6–8 ppm region, whereas the integrations met the expected structures. In ^{1}H NMR, compound **A3** showed two singlets at 1.32 and 2.57 ppm, according to integration (6H for each) confirming that the structure is symmetric for -1, -3, -5, -7 methyl protons on kryptopyrrole rings. Similarly, the peaks observed at 6.56, 6.58, and 6.52 ppm for **B3**,

B4, and **C3**, respectively, belong to the pyrrolic hydrogens at the positions -2 and -6 of the indacene structure, proving that all compounds are symmetric. Selective signals for compound **C3** belonging to the methoxy groups were observed as two singlet peaks at 3.31 and 3.84 ppm. Typically, there are noncrucial and presumable differences between the chemical shifts of pyrrolic ring protons of the compounds. Pyrrolic hydrogens (on the -β positions—on the pyrrole rings) were observed to shift to the upper field in ^{1}H NMR due to the presence of electron-donating methoxy groups (6.56 and 6.52 ppm for **B3** and **C3**, respectively). Although the electron-withdrawing chlorine substituent is at a distant *meso* (8) location, the value of the related protons shifted downfield (6.56 and 6.58 ppm for the **B3** and **B4**, respectively). Whilst the compounds **A2**, **B2**, and **C2** are not the intended BODIPYs, the chemical shift values of the aldehyde protons in these molecules could give preliminary information about the electron density and/or steric hindrance of the BODIPY core. A singlet was observed at 10.14, 9.66, and 9.71 ppm for the respective aldehyde protons of the **A2**, **B2,** and **C2**, respectively. Accordingly, the steric hindrance of the phenyl groups at the -1 and -7 positions of the compounds, combined with their shielding ring currents, increased the electron density of the core structure. In general, the FT-IR spectra of the resulting compounds (**A3**, **B3**, **B4,** and **C3**) exhibited various bands in the 650–4000 cm^{-1} spectral region. After forming the final compounds, the intense aldehyde carbonyl vibrations (C = O) at 1701 cm^{-1} (for **A2** and **B2**) and 1697 cm^{-1} (for **C3**) disappeared as expected. The intense aromatic structures show C-H stretching modes between 3000–3100 cm^{-1} while C = C vibrations were observed intensely in the region between 1500–1700 cm^{-1}. The aliphatic C–H stretching peaks are more prominent due to the methoxy groups below 3000 cm^{-1} for the **C3**. The C = N vibration peaks between 1546–1534 cm^{-1} were observed as weak or medium intensity. The intense B-F stretching vibrations were observed at 1190 cm^{-1} for the compound **A3** and at 1141 cm^{-1} for the rest (**B3**, **B4,** and **C3**), which shifts to lower frequencies due to the change of alkyl substituents on pyrrole rings to aryl groups. Various intensity peaks were assigned to ν_s (N-B) and ν_{as} (N-B) of the BODIPY core, in the vicinity of 1250 cm^{-1}. The HRMS was recorded based on an electrospray ionization time-of-flight (ESI-TOF) mode. The theoretical molecular masses of the structures were calculated by considering the isotopes (^{13}C, ^{14}C, ^{15}N, ^{16}O, ^{11}B, ^{10}B) found in their structures. The related peaks of the final compounds were observed as $[M+H]^+$ and $[M\text{-}H]^-$ molecular ion peaks. The errors in mass accuracy as ppm (Δ) calculated for the final compounds were found to be the highest as 4.06 and the lowest 0.70. The HRMS/TOF data validated that all constructs were consistent with their theoretical values.

Photophysical Properties

The absorption and fluorescence spectra of the investigated BODIPYs (**A3**, **B3**, **B4**, **C3**) were obtained in THF at room temperature. The related spectra of the final dyes are depicted in Fig. 3a-b. The full photophysical data were compiled in Table 1.

The absorption spectrum of **A3** as a reference that was obtained from the kryptopyrrole displayed the characteristic BODIPY profile with an intense and narrow absorption band at 529 nm belonging to the S_0-S_1 (π -π*) transition with a shoulder assigned to the 0 − 1 vibrational band of the same transition (Fig. 3a). The weaker and broader absorption bands were also seen at around

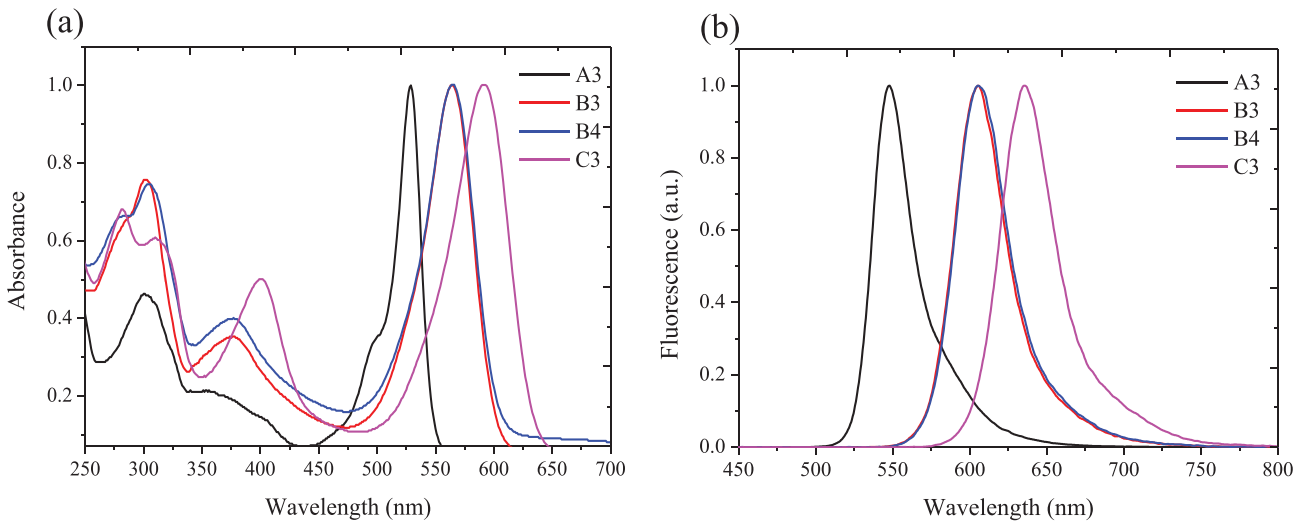

Fig. 3 Normalized **a** absorption and **b** fluorescence spectra of the BODIPYs (**A3**, **B3**, **B4** and **C3**) at room temperature

Table 1 Photophysical parameters of the BODIPYs in THF

Compound	λ_{abs} (max/nm)	λ_{ems} (max/nm)	ε (M^{-1} cm^{-1}) $\times 10^4$	FWHM (nm)	Stokes shifts Δv_{ss} (nm)	[a]Φ_F	[b]Φ_Δ
A3	529	548	4.66	26	19	0.58	0.084
B3	564	606	5.26	35	42	0.26	0.114
B4	565	606	5.84	55	41	0.23	0.078
C3	592	636	6.12	62	44	0.27	0.066

a: Fluorescein in ethanol ($\Phi_F = 0.79$) was used as the fluorescence standard for fluorescence quantum yield calculations and correction for the solvent refractive index (η) was applied [THF: η = 1.4072, EtOH: 1.3614]. b: Methylene blue ($\Phi_\Delta = 0.57$ in CH_2Cl_2) was used as reference compound for determining singlet oxygen quantum yields

375 nm corresponding to higher energy level transitions (S_0-S_2, etc.). When the absorption spectra of the starting BODIPYs (**A2**, **B2,** and **C2**) were compared with the resulting dyes (**A3**, **B3**, **B4** and **C3**), it was seen that the absorption bands at 300 nm belong to the 2-phenylbenzimidazole groups attached to the *meso* (8) carbon atoms of the BODIPY cores. Since the BODIPY indacene plane and the *meso* substituent are practically vertical to each other, as has been observed in BODIPY dyes [54, 55], no considerable spectral shifts were observed depending on the change of the substituent at the aforementioned position. In this way, the conjugation of the phenyl-benzimidazoles linked to the *meso* (8) position was hindered by the steric hindrance of this location, and the electronic properties of the substituents did not cause a shift in the absorption spectra. However, the presence of aryl groups instead of methyl/ethyl groups in closer proximity (-*α* and -*β* positions) significantly shifted the absorption wavelengths to the lower energy region. A bathochromic shift of 35 nm was observed with the presence of phenyl groups at the -1, -3, -5, and -7 positions of the BODIPY core. In addition to π—π* transitions originating from intense phenyl groups, the n—π* transitions within methoxyphenyl subunits amplify this effect. Consequently, the primary absorption band of **C3** manifests at 592 nm, exhibiting a bathochromic shift of 63 nm when compared to **A3**. Similarly, the peak at 375 nm increased and shifted to 400 nm due to the relevant transitions in the *p*-methoxyphenyl groups of **C3** (Fig. 3a).

The effects of the increased conjugation based on π-extended auxochrome groups in compounds **B3**, **B4,** and **B5** compared to **A3** were also reflected in their molar absorption coefficients (ε), Stokes shifts and spectral bandwidths (FWHM) that the specified parameters have increased systematically. When comparing **A3** and **C3**, the full width at half media value (FWHM) has increased from 26 to 62 nm, and the Stokes shift has increased from 19 to 44 nm. One of the major drawbacks of the BODIPYs is relatively small Stokes shifts that lead to loss of fluorescence due to self-quenching. Hence, the increased Stokes shifts emphasize the importance of the phenyl groups on the BODIPY core. The remarkable increases in absorption coefficients and spectral bandwidths reveal that arylated compounds absorb visible-region photons more effectively. Furthermore, due to the presence of aromatic phenyl groups, the intensity of transitions with higher energy centered at 300 and 375 nm also increased significantly for the compounds **B3** and **B4** (Fig. 3a).

The fluorescence spectra of the final BODIPYs exhibit a single band with a peak ranging from 548 to 636 nm when excited at the maximum absorption wavelengths. Notably, this fluorescence pattern mirrors the absorption spectra (Fig. 3b). The introduction of the phenyl/methoxyphenyl groups resulted in a bathochromic shift from 58 to 88 nm of the emission bands compared with compound **A3**. On the other hand, the fluorescence quantum yields of the **B3**, **B4,** and **C3** compounds were reduced by about half (Table 1) compared to methylated analog **A3,** suggesting that this phenomenon may be caused by non-radiative loss of energy via rotation around the C-Ar bonds and extended π conjugation [50, 56]. Therefore, the compounds fluoresce with a quantum yield (Φ_F) of 0.58 to 0.23, depending on the substitution of methyl/ethyl and phenyl/methoxyphenyl. The chlorine atom at the benzimidazole ring did not affect the fluorescence wavelength as it was located to distant *meso* (8) position of the BODIPY core, but slightly reduced the fluorescence quantum yield (0.26 and 0.23 for compounds **B3** and **B4**, respectively).

Due to the need for molecules that do not contain heavy atoms such as bromine in photodynamic therapy (PDT) applications, studies on the obtaining of new photosensitizers are increasing [57, 58]. Therefore, we further determined the singlet oxygen quantum yields ($\Phi_{\Delta)}$) of the dyes in dichloromethane (DCM) with 1,3-diphenylisobenzofuran (DPBF) as a chemical singlet oxygen trap. The absorption/photodegradation profiles of the compounds **A3**, **B3**, **B4,** and **C3** are shown in Fig. S1 and the related data are given in Table 1. A good linear relation between the DPBF absorbance at 414 nm against time indicated that the reaction kinetics were in zero order. As can be seen from the figures by comparison, the main absorbance bands of the

BODIPYs were nearly intact, while the absorption band of the DPBF at 414 nm was decreased perceptibly depending on the singlet oxygen production. Singlet oxygen quantum yields (Φ_Δ) of the compounds were calculated as 8.4%, 11.4%, 7.8%, and 6.6% for the compounds **A3**, **B3**, **B4,** and **C3**, respectively. Apparently, no significant differences were observed between the values found. The values obtained did not exhibit any significant differences. Unlike the compound **A3**, which features methyl and ethyl substituents, the substitution of phenyl subunits led to an approximately 30% increase in Φ_Δ values. Although the quantum yields of the compounds were moderate, they were lower compared to their triplet-forming analogs containing heavy atoms such as bromine and iodine [57, 59, 60]. However, due to the presence of -1, -3, -5, and -7 aryl groups, the light absorption of the molecules has increased in the visible spectral range. Furthermore, this configuration facilitates excitation with lower energy.

Computational Studies on Photophysical Properties of the Compounds

The computational approach of DFT has been widely used to elaborate the photophysical properties of BODIPY dyes, as it gives compatible results with experimental ones [30, 36, 38–42, 61]. Therefore, to rationalize the photophysical properties of the compounds studied, we performed calculations using DFT/TD-DFT methods. The theoretical data that include dipole moments (μ), the first two electronic excitation energies (E_v), corresponding oscillator strengths (f), and the main configurations are summarized in Table 2. The optimized structures and the density of states (DOS) spectra showing the frontier molecular orbital energies of the investigated BODIPYs are demonstrated in Fig. 4.

The molecular geometry optimizations showed that the BODIPY core takes planar geometry and the complexes adopt pseudo tetrahedral geometry. Such that the angles between the F-B-F atoms for all compounds vary between 107–108°, and those between the N-B-N atoms vary between 107–109°. The dihedral angle between the BODIPY moiety and the 2-phenylbenzimidazole group at the *meso* position was estimated as 88º for compound **A3**, while the relevant angles of the rest were 64 ~ 65º. The angle between the two conjugated groups decreased due to the sterical effect of aryl groups in the α (-3, -5) and β (-1, -7) positions of the core. This may partially increase the π-π interactions between the two planes. Also, all the final BODIPYs have polar character, and the dipole moments were 7.59 and 6.53 for the compound **A3** and its phenyl-substituted analog **B3**, respectively. The molecular dipole moments were oriented from the BODIPY core to the *meso* (8) substituents. The electronegative chlorine atom at the *meso* position significantly equalized the dipole moment of the **B4** molecule. Therefore, the dipole moment of the compound **B4** decreased to 2.95 debye, and the polarity of the molecule reduced. The change of frontier orbital energies of HOMO and LUMO were analyzed by density of states (DOS) diagrams, which were drawn by plotting molecular orbital data of the investigated compounds (Fig. 4).

Although there were no drastic changes in DOS spectra, the energy levels of the frontier molecular orbitals approach each other depending on the presence of the phenyl and *p*-methoxyphenyl substituents. The main transitions were between HOMO → LUMO (contribution 91–98%) due to electronic excitations from the S_0-S_1 energy levels. The energy band gaps ($\Delta E = |E_{HOMO} - E_{LUMO}|$) were calculated to be 2.74 eV, 2.37 eV, 2.37 eV and 2.17 eV for the compounds **A3**, **B3**, **B4,** and **C3**, respectively, reflecting decreased transition energies, which were in good agreement with the red-shifted absorption spectra. In other words, with, the energy gap between HOMO and LUMO decreased due to the presence of aromatic phenyl groups, leading to longer absorption wavelength maximums for the compounds **B3**, **B4,** and **C3**. Besides, the chlorine atom in a distant position of the *meso* substituent did not affect the HOMO/LUMO energy levels of the compound **B4**. The calculated singlet excitation energies (E_E) which constitute the

Table 2 Dipole moments (μ), Electronic excitation energies (E_v), Corresponding oscillator strengths (*f*) and the main configurations of the low-lying electronic excited states of the compounds

Compound	Dipole moment μ/ Debye	Vertical excitation energy eV/nm	Oscillator strength *f*	Major contribution
A3	7.59	2.74 / 452 3.28 / 378	0.57 0.21	HOMO → LUMO (93%) H – 1 → LUMO (91%)
B3	6.53	2.37 / 522 2.45 / 507	0.68 0.19	HOMO → LUMO (91%) H – 1 → LUMO (88%)
B4	2.95	2.37 / 522 2.52 / 492	0.75 0.10	HOMO → LUMO (98%) H – 1 → LUMO (93%)
C3	5.95	2.17 / 572 2.35 / 527	0.79 0.02	HOMO → LUMO (98%) H – 1 → LUMO (97%)

Compound	Optimized structure	Density of states (DOS)
A3	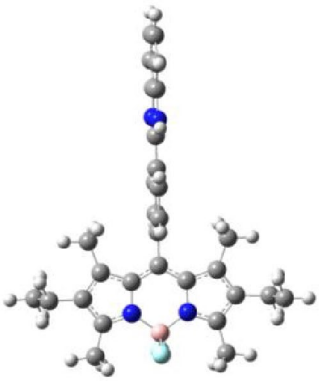	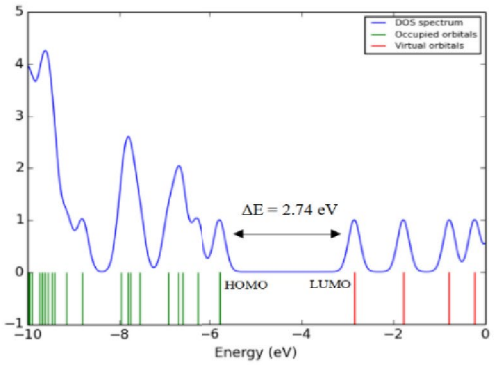
B3	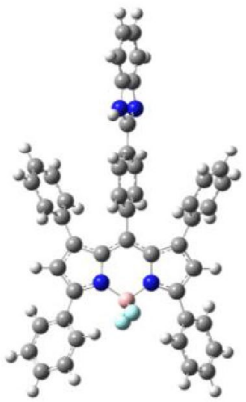	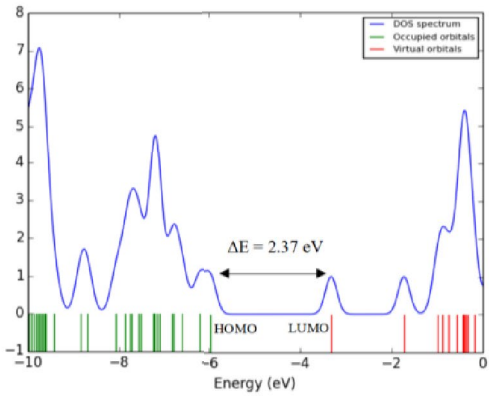
B4	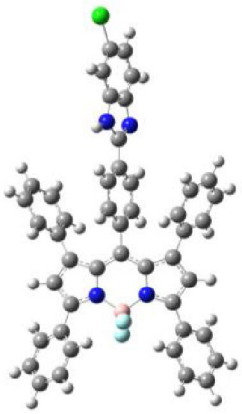	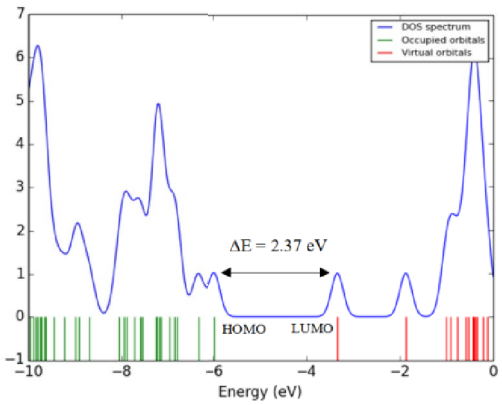
C3	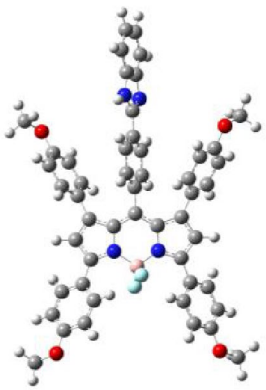	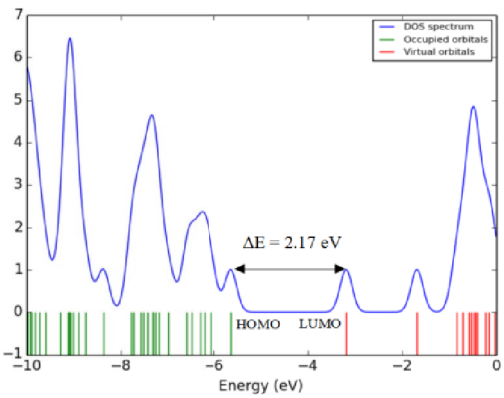

Fig. 4 Optimized structures and Density of states (DOS) spectra of the BODIPYs

absorption spectra (λ_{cal}) by the TDDFT method validated the experimental values (λ_{exp}). Such that, $\lambda_{exp}/\lambda_{cal}$ ratios of the main absorption bands were calculated as 1.17, 1.08, 1.08, and 1.03 for the **A3**, **B3**, **B4,** and **C3**, respectively. The HOMO–LUMO gap (ΔE) is an indicator of the chemical hardness–softness of a molecule that is small for soft molecules and large for hard molecules. According to the calculated values between 2.74–2.17 eV, all final BODIPYs could be considered soft molecules.

To have a better visualization of the electronic transitions, natural transition orbitals (NTOs) were calculated, which is a combined representation of the excited electron–hole pairs obtained from the transition density matrices calculated by TDDFT [62, 63]. The related NTOs and centroids of hole and electron isosurfaces for the lowest energy transitions ($S_0 \rightarrow S_1$) of the dyes are given in Table 3.

In the transition orbital isosurfaces, the main distribution regions of the electron and hole correspond to the green and blue, respectively. Calculations showed that both excited electrons and holes located in the BODIPY core mainly correspond to the HOMO and LUMO, respectively. The electrons for the main transition (S_0-S_1) states were exclusively localized on the BODIPY core, while the holes were partially spread on the substituents at the -1, -3, -5, -7, and -8 (*meso*) positions. In particular, the orbital distributions of both electron and hole were in the -3 and -5 positions, indicating the uninterrupted conjugation of these positions with the BODIPY core. However, the electron density on the phenyl rings at positions -1, -7, and -8 (*meso*) was of practically low importance. It was seen that auxochrome methoxy groups also contribute to the electron for **C3**, which supported the decrease in excitation energy (E_E), and thus the bathochromic effect in the UV–vis spectrum. The centroids of hole and electron (C_{hole} & C_{ele}) made the electron/hole distribution behavior smoother (Table 3). Accordingly, the electron and hole pairs overlap to a large extent. Here, the *t* index is a numerical value that indicates the separation of the hole-electron couple. $t > 0$ means the hole/electron separation is clear. However, inferring from Table 3, the *t* values were negative in all directions for the investigated BODIPYs, reflecting that the holes and electron counterparts overlap severely with each other. Similarly, all the molecules showed higher Coulomb attractive energies (E_c, exciton binding energies), that reduce the exciton dissociations between the holes and electrons in comparison to transition energies (E_E). Therefore, we can conclude that the S_0-S_1 transitions include substantially the local excitations with n–π and π -π* feature. Electrons due to these transitions were more dominantly localized in the BODIPY core. The main absorption bands observed in the experimental absorption spectra of the compounds belong to the corresponding transitions.

Thermal Properties

The thermal stability of dyes may limit their use in various systems. Therefore, the thermal properties of the resulting compounds were characterized by thermogravimetric analysis (TGA). The thermal stability of the compounds has been described by several quantifications. The thermal degradation graphs of the compounds are given in Fig. 5 and the thermogram parameters are given in Table 4. It was observed that compounds in an inert N_2 atmosphere have demonstrated initial thermal stability up to temperatures exceeding 300 °C. A mass loss of 3% at 87 °C was observed due to desorption of water for only **A3**.

Compounds generally have a dominant two-step decay in the range of 312–620 °C, except for **C3**. In the range of 300–1100 °C, lower rate and mass loss degradation phases were observed, which may be associated with the gradual breaking of covalent bonds in the structures and carbonization of organic groups in the BODIPY skeleton. Compound **A3**, which includes kryptopyrrole, degrades rapidly at 355 °C with a decomposition rate of 14.8 (% / min), while the primary degradation of **B3**, analog with phenyl groups, takes place at a lower rate (5.1% / min) at 349 °C. The thermal stability of the compounds is in the form of **C3** > **B3** > **A3** > **B4**, and it can be stated that the methoxyphenyl and phenyl groups in the indacene rings enhance the thermal stability, whereas the chlorine atoms in the *meso* (8) position of the core structure diminish it. It was observed that the thermal stabilities increase slightly when K-BDP as reference compound, which has a phenyl ring in the *meso* position and kryptopyrrole groups in indacene core, is taken as a reference. It has been observed that the first stage of decomposition, especially covering 300–350 °C, occurs at higher temperatures. Except for **C3**, all compounds were charred totally at 1100 °C. For organic compounds, the carbonization efficiencies (%) at 700 °C are typically taken as a base, and they are 82, 75, 61, 84 and 38, for the reference BODIPY and **A3-C3**, respectively.

Biological Properties

The antibacterial activities of the resulting compounds are presented as agar spot plating. The treatments with the compounds did not cause any inhibitory effect on *Pseudomonas aeruginosa* 27,853, since there is a similar trend of inhibition between the studied compounds and only DMSO solvent control (Figs. S37-S40). It is important to mention that DMSO is employed for dissolving the compounds and thus utilized as an experimental control. The antibacterial and antibiofilm actions of DMSO have been documented previously [64–66]. On the other hand, all the compounds demonstrated antibacterial effects at 1.0 mg / mL concentration against *Escherichia coli* 35,218, as their

Table 3 Natural transition orbitals for the lowest-energy transitions of the BODIPYs (isosurface value = 0.02 au), centroids of hole and electron (C_{hole} & C_{ele})

Compound	Transition	Electron	Hole	C_{hole} & C_{ele}
A3	S_0-S_1 E_E: 2.74 eV *f* = 0.57 *t* (Å): -0.848 E_C: 5.24 eV	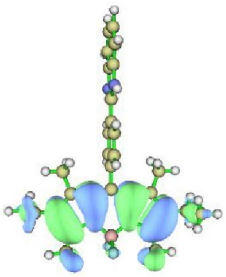	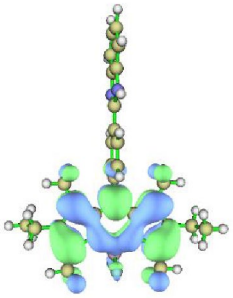	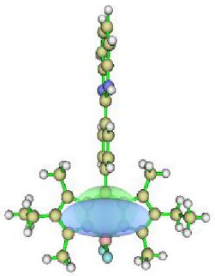
B3	S_0-S_1 2.37 eV *f* = 0.68 *t* (Å): -2.332 E_C: 3.86 eV	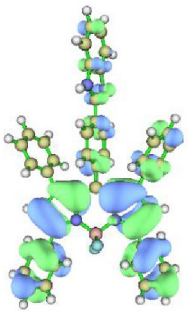	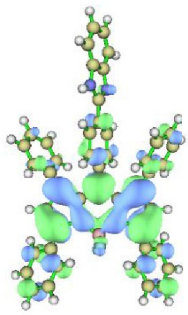	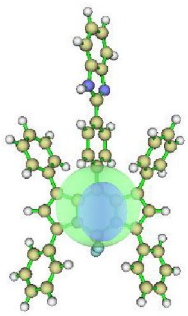
B4	S_0-S_1 2.37 eV *f* = 0.75 *t* (Å): -1.451 E_C: 4.03 eV	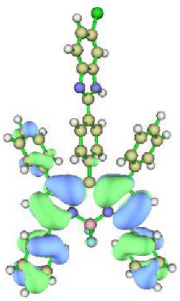	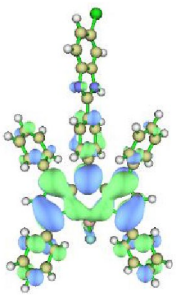	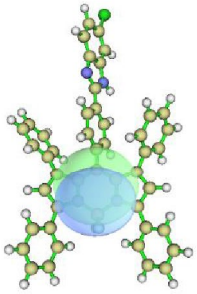
C3	S_0-S_1 2.17 eV *f* = 0.79 *t* (Å): -1.395 E_C: 3.59 eV	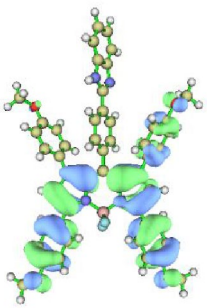	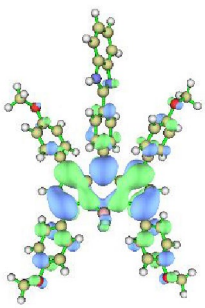	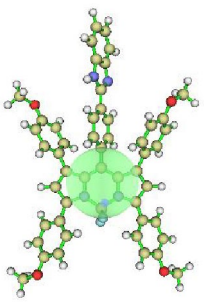

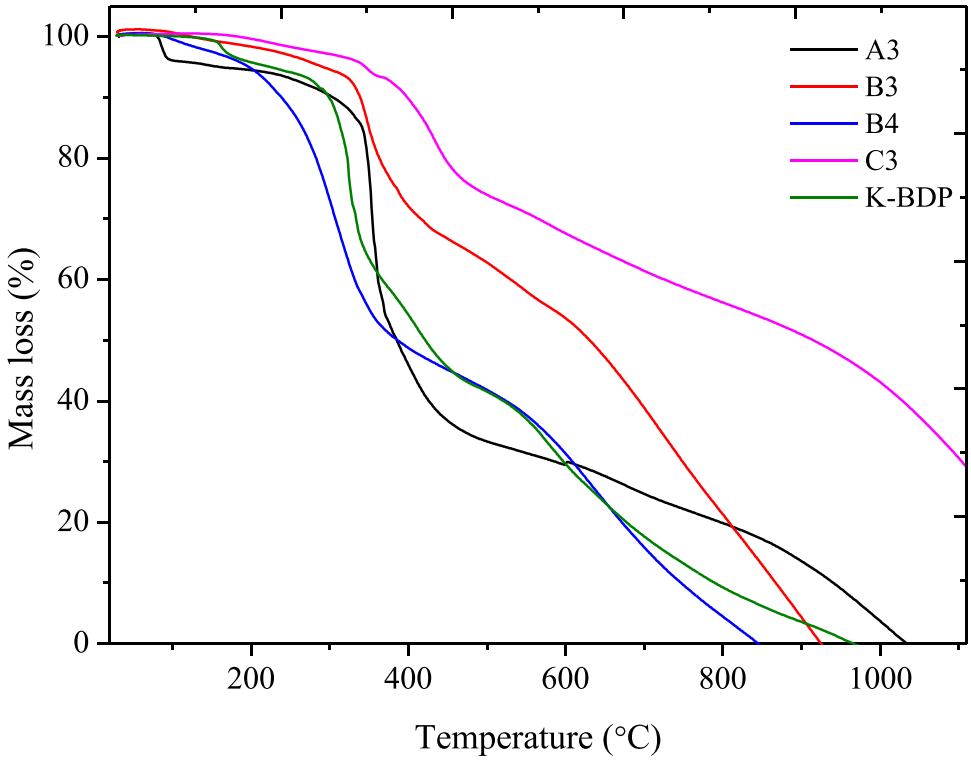

Fig. 5 Thermogram of the compounds at a temperature ramp of 10 °C/min under N_2

inhibitory action exceeded that of DMSO (Figs. S33-S36). The biofilm-formation event in *P. aeruginosa* 27,853 and *E. coli* 35,218 strains were also investigated using a CV staining assay and quantitative changes are presented in Figs. 6 and S37. The compounds **C3** and **B3** exhibited anti-biofilm effects on both types of bacteria within the dosage range of 0.5–2.0 mg / mL. DMSO also displayed its own inhibitory effect, but the inhibitory potency of these compounds was notably stronger (Fig. 6). Nevertheless, the anti-biofilm potency of compound **B4** was comparable to that of DMSO and was consequently deemed insignificant (Fig. S41).

Table 4 The decomposition temperatures and thermal stability of the compounds

Compound	T_{max} (°C)*	Mass loss (%)	Decomposition rate (%/min)	**T10% (°C)	T30% (°C)	T50% (°C)
K-BDP	325	24	16.1	300	340	430
	413	49	1.5			
	577	64	2.2			
A3	355	32	14.8	303	354	384
	411	57	2.4			
B3	349	15	5.1	339	415	630
	545	41	1.1			
B4	312	32	4.5	238	306	386
	620	72	1.6			
C3	346	6	1.0	398	564	915
	430	16	2.6			
	580	31	0.7			

*Maximum decomposition temperatures based on DTG plot; ** T10% (temperature at which 10% of initial mass is lost), etc

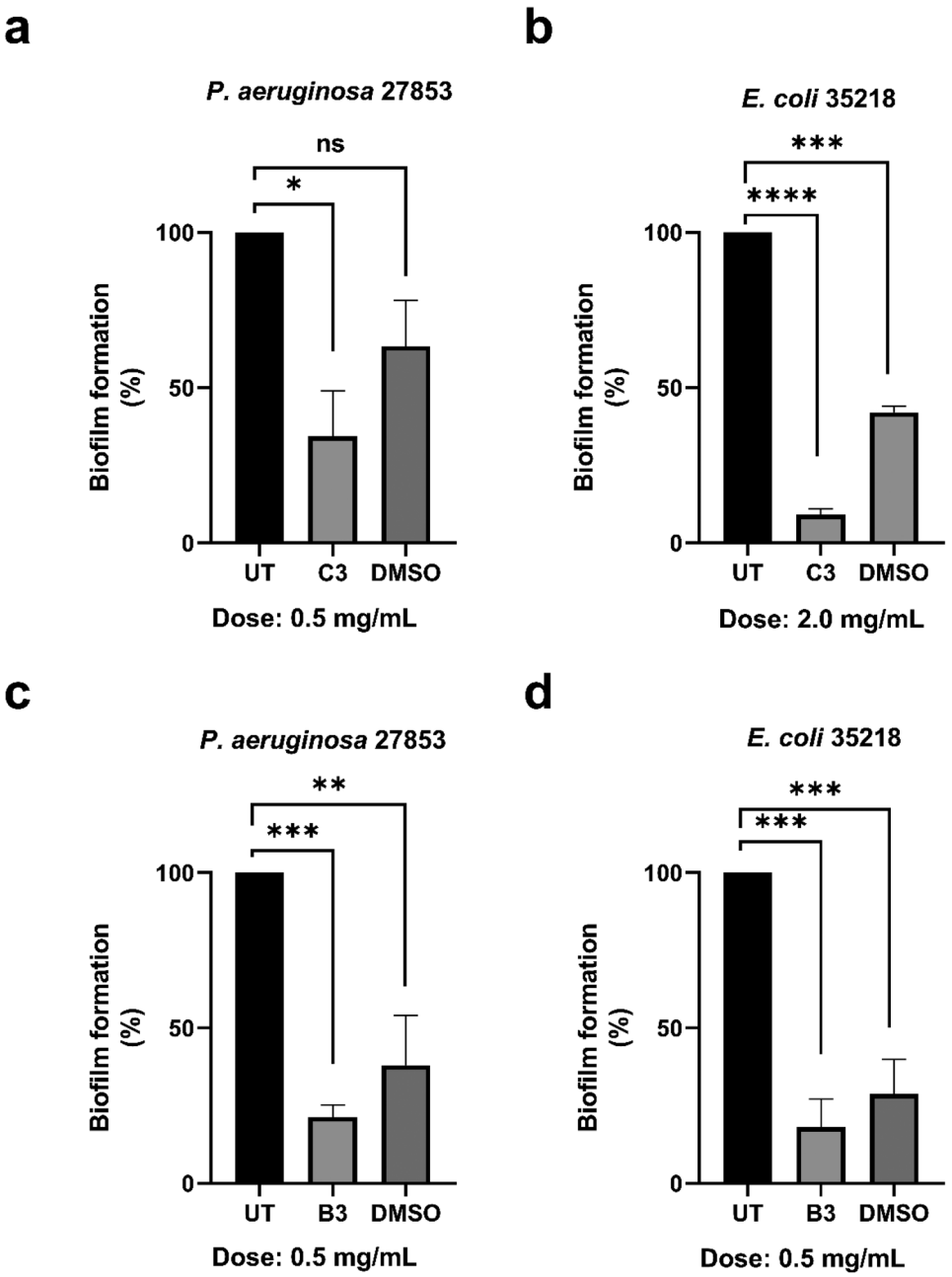

Fig. 6 Anti-biofilm activities of the compounds **C3** (**a**-**b**) and **B3** (**c**-**d**) on biofilm-forming *Pseudomonas aeruginosa* 27,853 and *Escherichia coli* 35,218. The biofilm development was examined through a crystal violet (CV) staining assay. Quantitative results are presented as percentages (%). DMSO was used as a solvent control. The experiments were conducted multiple times independently, with a minimum of two repetitions, each involving technical replicates. ns: non-significant, *$p \leq 0.05$; **$p \leq 0.01$; ***$p \leq 0.001$; ****$p \leq 0.0001$. UT: untreated

Conclusions

In summary, benzimidazole-appended BODIPY derivatives were successfully synthesized via formyl group on the *meso* position of the BODIPYs under mild conditions and characterized chemically. It was determined that the use of 2,4-diaryl substituted pyrrole derivatives in the synthesis of BODIPYs increases the synthetic yields. Differences in the functional phenyl and methoxyphenyl substitution of distal and proximal positions of the pyrrole rings rather than methyl/ethyl groups noticeably affected the basic photophysical properties of the BODIPYs. The presence of aryl groups at the -1, -3, -5, and -7 positions of the BODIPY core was accompanied by substantial increases (up to 63 nm) in the bathochromic shift of the main absorption band compared to the methylated analog. The enhancement of conjugation increased the photophysical parameters such as molar absorption coefficients, Stokes shifts, and spectral bandwidths (FWHM). The $^1O_2$ formation abilities of the compounds were also determined by a comparative method with a singlet oxygen trap molecule. In terms of singlet oxygen quantum yields (Φ_Δ), the investigated compounds exhibited the lower photodynamic activities ranging from ~ 7% to ~ 11% compared to analogues containing heavy atoms

through enhanced spin–orbit coupling. To better understand molecular orbital excitation properties, DFT and TD-DFT computations were conducted. Theoretical calculations indicated that the $S_0 \rightarrow S_1$ transitions were nearly pure and corresponded to the HOMO to LUMO transitions. The electron–hole analysis revealed that the aforementioned counterparts exhibit strong overlap with each other. Thus, both electrons and holes for the main transitions were exclusively localized on the BODIPY core. Moreover, the compounds were determined to be thermostable and had mainly two-stage decomposition behavior in the range of 312–620 °C based on the TGA in an inert N_2 atmosphere. While the *p*-methoxyphenyl and phenyl groups in the indacene rings increased thermal stability, the chlorine atoms in the *meso* (*8*) position of the BODIPY core decreased. Furthermore, the compounds were effective against *E. coli* bacteria at a concentration of 1.0 mg/mL. Additionally, compounds C3 and B3 inhibited the biofilms of *P. aeruginosa* and *E. coli* at concentrations between 0.5 and 2.0 mg / ml. The findings are expected to contribute to BODIPY research and provide valuable insights for improving BODIPY chromophores.

Supplementary Information The online version contains supplementary material available at https://doi.org/10.1007/s10895-024-03688-8.

Author Contributions Gökhan Sevinç: Writing - Review & Editing, Supervision, Methodology Emine Doğan: Investigation, Writing - Review & Editing, Data Curation Sina Mansuroğlu: Investigation, Writing - Review & Editing, Data Curation Rafig Gurbanov: Writing - Review & Editing, Supervision, Methodology

Funding The authors declare that no funds, grants, or other support were received during the preparation of this manuscript.

Data Availability The data used and/or analyzed in the current study are provided in the submitted article.

Declarations

Ethics Approval N/A.

Competing Interests The authors declare no competing interests.

References

1. Singh SP, Gayathri T (2014) Evolution of BODIPY dyes as potential sensitizers for dye-sensitized solar cells. European J Org Chem 2014:4689–4707
2. Yildiz EA, Sevinc G, Yaglioglu HG, Hayvali M (2019) Strategies towards enhancing the efficiency of BODIPY dyes in dye sensitized solar cells. J Photochem Photobiol A Chem 375:148–157
3. Mao M, Song Q (2016) The structure-property relationships of D-π-A bodipy dyes for dye-sensitized solar cells. Chem Rec 16:719–733
4. Telore RD, Jadhav AG, Sekar N (2016) NLOphoric and solid state emissive BODIPY dyes containing N-phenylcarbazole core at meso position–synthesis, photophysical properties of and DFT studies. J Lumin 179:420–428
5. Mallah RR, Mohbiya DR, Sreenath MC, Chitrambalam S, Joe IH, Sekar N (2019) Non-linear optical response of meso substituted dipyrromethene boron difluoride dyes: Synthesis, photophysical, DFT and Z scan study. Opt Mater (Amst) 89:164–172. https://doi.org/10.1016/J.OPTMAT.2019.01.025
6. Thakare SS, Sreenath MC, Chitrambalam S, Joe IH, Sekar N (2017) Non-linear optical study of BODIPY-benzimidazole conjugate by solvatochromic. Z-scan and theoretical methods Opt Mater (Amst) 64:453–460. https://doi.org/10.1016/J.OPTMAT.2017.01.020
7. Nguyen V, Yim Y, Kim S, Ryu B, Swamy KMK, Kim G et al (2020) Molecular design of highly efficient heavy-atom-free triplet BODIPY derivatives for photodynamic therapy and bioimaging. Angew Chem Int Ed 59:8957–8962
8. Kaur P, Singh K (2019) Recent advances in the application of BODIPY in bioimaging and chemosensing. J Mater Chem C Mater 7:11361–11405
9. Kursunlu AN, Guler E (2014) The sensitivity and selectivity properties of a fluorescence sensor based on quinoline-Bodipy. J Lumin 145:608–614
10. Xia H-C, Xu X-H, Song Q-H (2017) BODIPY-based fluorescent sensor for the recognization of phosgene in solutions and in gas phase. Anal Chem 89:4192–4197
11. Tang F-K, Zhu J, Kong FK-W, Ng M, Bian Q, Yam VW-W et al (2020) A BODIPY-based fluorescent sensor for the detection of Pt2+ and Pt drugs. Chem Commun 56:2695–2698
12. Liu M, Ma S, She M, Chen J, Wang Z, Liu P et al (2019) Structural modification of BODIPY: Improve its applicability. Chin Chem Lett 30:1815–1824
13. Li F-Z, Yin J-F, Kuang G-C (2021) BODIPY-based supramolecules: Construction, properties and functions. Coord Chem Rev 448:214157
14. Poddar M, Misra R (2020) Recent advances of BODIPY based derivatives for optoelectronic applications. Coord Chem Rev 421:213462
15. Rocha-Ortiz JS, Insuasty A, Madrid-Usuga D, Mora-León AG, Ortiz A (2021) Optical and electrochemical effects of triarylamine inclusion to alkoxy BODIPY-based derivatives. New J Chem 45:18114–18123. https://doi.org/10.1039/D1NJ02610K
16. Rocha-Ortiz JS, Montalvo-Acosta JJ, He Y, Insuasty A, Hirsch A, Brabec CJ et al (2023) Structure and linkage assessment of T-shaped Pyrrolidine[60]Fullerene- and Isoxazoline[60]Fullerene-BODIPY-triarylamine hybrids. Dyes Pigments 217:111445. https://doi.org/10.1016/j.dyepig.2023.111445
17. Rocha-Ortiz JS, Wu J, Wenzel J, Bornschlegl AJ, Perea JD, Leon S et al (2023) Enhancing Planar Inverted Perovskite Solar Cells with Innovative Dumbbell-Shaped HTMs: A Study of Hexabenzocoronene and Pyrene-BODIPY-Triarylamine Derivatives. Adv Funct Mater 33:2304262. https://doi.org/10.1002/adfm.202304262
18. Banfi S, Nasini G, Zaza S, Caruso E (2013) Synthesis and photophysical properties of a series of BODIPY dyes. Tetrahedron 69:4845–4856
19. Clarke RG, Hall MJ (2019) Recent developments in the synthesis of the BODIPY dyes. Adv Heterocycl Chem 128:181–261. https://doi.org/10.1016/BS.AIHCH.2018.12.001
20. Sánchez-Arroyo AJ, Palao E, Agarrabeitia AR, Ortiz MJ, García-Fresnadillo D (2017) Towards improved halogenated BODIPY photosensitizers: clues on structural designs and heavy atom substitution patterns. Phys Chem Chem Phys 19:69–72
21. Fan G, Yang L, Chen Z (2014) Water-soluble BODIPY and aza-BODIPY dyes: synthetic progress and applications. Front Chem Sci Eng 8:405–417
22. Buyukcakir O, Bozdemir OA, Kolemen S, Erbas S, Akkaya EU (2009) Tetrastyryl-Bodipy dyes: convenient synthesis and characterization of elusive near IR fluorophores. Org Lett 11:4644–4647

23. Hayashi Y, Yamaguchi S, Cha WY, Kim D, Shinokubo H (2011) Synthesis of directly connected BODIPY oligomers through Suzuki-Miyaura coupling. Org Lett 13:2992–2995
24. Rohand T, Qin W, Boens N, Dehaen W (2006) Palladium-Catalyzed Coupling Reactions for the Functionalization of BODIPY Dyes with Fluorescence Spanning the Visible Spectrum. Eur J Org Chem 2006:4658–4663. https://doi.org/10.1002/ejoc.200600531
25. Pathare B, Bansode T (2021) Review- biological active benzimidazole derivatives. Results Chem 3:100200. https://doi.org/10.1016/j.rechem.2021.100200
26. Brishty SR, Hossain MJ, Khandaker MU, Faruque MRI, Osman H, Rahman SM (2021) A comprehensive account on recent progress in pharmacological activities of benzimidazole derivatives. Front Pharmacol 12:762807
27. Tahlan S, Kumar S, Narasimhan B (2019) Pharmacological significance of heterocyclic 1H-benzimidazole scaffolds: a review. BMC Chem. https://doi.org/10.1186/s13065-019-0625-4
28. Hashem HE, El Bakri Y (2021) An overview on novel synthetic approaches and medicinal applications of benzimidazole compounds. Arab J Chem 14:103418. https://doi.org/10.1016/j.arabjc.2021.103418
29. Madhu S, Ravikanth M (2014) Boron-Dipyrromethene Based Reversible and Reusable Selective Chemosensor for Fluoride Detection. Inorg Chem 53:1646–1653. https://doi.org/10.1021/ic402767j
30. Li Z, Li L-J, Sun T, Liu L, Xie Z (2016) Benzimidazole-BODIPY as optical and fluorometric pH sensor. Dyes Pigments 128:165–169. https://doi.org/10.1016/j.dyepig.2016.01.029
31. Madhu S, Sharma DK, Basu SK, Jadhav S, Chowdhury A, Ravikanth M (2013) Sensing Hg(II) in Vitro and in Vivo Using a Benzimidazole Substituted BODIPY. Inorg Chem 52:11136–11145. https://doi.org/10.1021/ic401365x
32. Gonçalves RCR, Pinto SCS, Costa SPG, Raposo MMM (2022) Anion Colorimetric Chemosensor Based on a Benzimidazole-Functionalized BODIPY Derivative. Chem Proc. https://doi.org/10.3390/ecsoc-25-11754
33. Chakraborty G, Ray AK, Singh PK, Pal H (2019) Non-covalent interaction of BODIPY-benzimidazole conjugate with bovine serum albumin–A photophysical and molecular docking study. J Photochem Photobiol A Chem 377:220–227. https://doi.org/10.1016/j.jphotochem.2019.04.001
34. Chakraborty G, Chattaraj S, Pal H (2023) pH assisted modulation in the binding affinity for BODIPY-benzimidazole conjugate with anionic cyclodextrin. J Photochem Photobiol A Chem 434:114266. https://doi.org/10.1016/j.jphotochem.2022.114266
35. Saiyasombat W, Nuchpun S, Katewongsa KP, Pornsuwan S, Weigand JJ, Kiatisevi S (2022) A turn-on bis-BODIPY chemosensor for copper recognition based on the in situ generation of a benzimidazole–triazole receptor and its applications in bioimaging. New J Chem 46:22525–22532. https://doi.org/10.1039/D2NJ04508G
36. Sevinç G, Küçüköz B, Yılmaz H, Şirikçi G, Yaglioglu HG, Hayvalı M et al (2014) Explanation of pH probe mechanism in borondipyrromethene-benzimidazole compound using ultrafast spectroscopy technique. Sens Actuators B Chem 193:737–744. https://doi.org/10.1016/j.snb.2013.12.043
37. Sevinç G, Hayvalı M (2018) The synthesis of new aryl borondipyrromethene compounds: Photophysical and pH responsive properties. J Turkish Chem Soc A: Chem 5:433–444. https://doi.org/10.18596/jotcsa.372452
38. Küçüköz B, Sevinç G, Yildiz E, Karatay A, Zhong F, Yılmaz H et al (2016) Enhancement of two photon absorption properties and intersystem crossing by charge transfer in pentaaryl borondipyrromethene (BODIPY) derivatives. Phys Chem Chem Phys 18:13546–13553
39. Matveeva MD, Zheleznova TYu, Kostyuchenko AS, Miftyakhova AR, Zhilyaev DI, Voskressensky LG et al (2023) 1,7-isoxazolyl Substituted BODIPY Dyes – Synthesis and Photophysical Properties. ChemistrySelect 8:e202204465. https://doi.org/10.1002/slct.202204465
40. Yildiz EA, Ünlü BA, Karatay A, Bozkurt Y, Özler ME, Sözmen F et al (2023) Two-photon absorption response of functionalized BODIPY Dyes in Near-IR Region by Tuning Conjugation Length and Meso-Substituents. ACS Omega 8:30939–30948. https://doi.org/10.1021/acsomega.3c02314
41. Helal W, Marashdeh A, Alkhatib Q, Qashmar H, Gharaibeh M, Afaneh AT (2022) Tuning the photophysical properties of BODIPY dyes used in DSSCs as predicted by double-hybrid TD-DFT: The role of the methyl substituents. Int J Quantum Chem 122:e27000. https://doi.org/10.1002/qua.27000
42. Mohajeri A, Kheshti T (2023) Improving the efficiency of dye-sensitized solar cells based on BODIPY dye and its analogous: The synergistic effect of benzo fusion and phenyl substitution. J Photochem Photobiol A Chem 442:114781. https://doi.org/10.1016/j.jphotochem.2023.114781
43. Frisch MJ, Trucks GW, Schlegel HB, Scuseria GE, Robb MA, Cheeseman JR et al (2009) Gaussian09 (Wallingford, CT: Gaussian, INC.)
44. Frisch R, Trucks GW, Schlegel HB, Scuseria GE, Robb MA, Cheeseman JR et al (2009) Gaussian 09, Revision E.01, 1 121, Gaussian, Inc., Wallingford CT
45. Lu T, Chen F (2012) Multiwfn: A multifunctional wavefunction analyzer. J Comput Chem 33:580–592. https://doi.org/10.1002/jcc.22885
46. O'boyle NM, Tenderholt AL, Langner KM (2008) cclib: A library for package-independent computational chemistry algorithms. J Comput Chem 29:839–45. https://doi.org/10.1002/jcc.20823
47. Hammadi Al-Ogaidi DA, Karaçam S, Gurbanov R, Vardar-Yel N (2024) Marine Microalgae Schizochytrium sp. S31: Potential Source for New Antimicrobial and Antibiofilm Agent. Curr Pharm Biotechnol. https://doi.org/10.2174/0113892010291960240223054911
48. Karadağ H, Tunçer S, Karaçam S, Gurbanov R (2022) Tapioca starch and skim milk support probiotic efficacy of Lactiplantibacillus plantarum post-fermentation medium against pathogens and cancer cells. Arch Microbiol 204:331. https://doi.org/10.1007/s00203-022-02943-5
49. Gurbanov R, Karadağ H, Karaçam S, Samgane G (2021) Tapioca Starch Modulates Cellular Events in Oral Probiotic Streptococcus salivarius Strains. Probiotics Antimicrob Proteins 13:195–207. https://doi.org/10.1007/s12602-020-09678-z
50. Sevinç G, Küçüköz B, Elmalı A, Hayvalı M (2020) The synthesis of −1, −3, −5, −7, −8 aryl substituted boron-dipyrromethene chromophores: Nonlinear optical and photophysical characterization. J Mol Struct 1206:127691. https://doi.org/10.1016/j.molstruc.2020.127691
51. Loudet A, Burgess K (2007) BODIPY dyes and their derivatives: Syntheses and spectroscopic properties. Chem Rev 107:4891–4932. https://doi.org/10.1021/cr078381n
52. Taşkıran ZP, Sevinç G (2022) Photophysical characterization of novel dipyrrine compounds based on pyrrolic hydrogen transfer. J Mol Struct 1260:132794. https://doi.org/10.1016/j.molstruc.2022.132794
53. Wood TE, Thompson A (2007) Advances in the chemistry of dipyrrins and their complexes. Chem Rev 107:1831–1861
54. Kollmannsberger M, Gareis T, Heinl S, Daub J, Breu J (1997) Electrogenerated Chemiluminescence and Proton-Dependent Switching of Fluorescence: Functionalized Difluoroboradiaza-s-indacenes. Angew Chem Int Ed Engl 36:1333–1335. https://doi.org/10.1002/anie.199713331
55. Werner T, Huber C, Heinl S, Kollmannsberger M, Daub J, Wolfbeis OS (1997) Novel optical pH-sensor based on a boradiaza-indacene derivative. Fresenius J Anal Chem 359:150–154. https://doi.org/10.1007/s002160050552

56. Cheng H, Cao X, Zhang S, Zhang K, Cheng Y, Wang J et al (2023) BODIPY as a multifunctional theranostic reagent in biomedicine: self-assembly, properties, and applications. Adv Mater 35:2207546
57. Wang J, Gong Q, Jiao L, Hao E (2023) Research advances in BODIPY-assembled supramolecular photosensitizers for photodynamic therapy. Coord Chem Rev 496:215367. https://doi.org/10.1016/j.ccr.2023.215367
58. Prieto-Castañeda A, García-Garrido F, Díaz-Norambuena C, Escriche-Navarro B, García-Fernández A, Bañuelos J et al (2022) Development of geometry-controlled all-orthogonal BODIPY trimers for photodynamic therapy and phototheragnosis. Org Lett 24:3636–3641. https://doi.org/10.1021/acs.orglett.2c01169
59. Awuah SG, You Y (2012) Boron dipyrromethene (BODIPY)-based photosensitizers for photodynamic therapy. RSC Adv 2:11169–11183. https://doi.org/10.1039/C2RA21404K
60. Kamkaew A, Lim SH, Lee HB, Kiew LV, Chung LY, Burgess K (2013) BODIPY dyes in photodynamic therapy. Chem Soc Rev 42:77–88. https://doi.org/10.1039/C2CS35216H
61. Buyuktemiz M, Duman S, Dede Y (2013) Luminescence of BODIPY and Dipyrrin: An MCSCF Comparison of Excited States. J Phys Chem A 117:1665–1669. https://doi.org/10.1021/jp311939s
62. Martin RL (2003) Natural transition orbitals. J Chem Phys 118:4775–4777. https://doi.org/10.1063/1.1558471
63. Liu B, Monro S, Jabed MA, Cameron CG, Colón KL, Xu W et al (2019) Neutral iridium(iii) complexes bearing BODIPY-substituted N-heterocyclic carbene (NHC) ligands: synthesis, photophysics, in vitro theranostic photodynamic therapy, and antimicrobial activity. Photochem Photobiol Sci 18:2381–2396. https://doi.org/10.1039/C9PP00142E
64. Ansel HC, Norred WP, Roth IL (1969) Antimicrobial Activity of Dimethyl Sulfoxide Against Escherichia coli, Pseudomonas aeruginosa, and Bacillus megaterium. J Pharm Sci 58:836–839. https://doi.org/10.1002/jps.2600580708
65. Summer K, Browne J, Hollanders M, Benkendorff K (2022) Out of control: The need for standardised solvent approaches and data reporting in antibiofilm assays incorporating dimethyl-sulfoxide (DMSO). Biofilm 4:100081. https://doi.org/10.1016/j.bioflm.2022.100081
66. Tunçer S, Gurbanov R (2023) Non-growth inhibitory doses of dimethyl sulfoxide alter gene expression and epigenetic pattern of bacteria. Appl Microbiol Biotechnol 107:299–312. https://doi.org/10.1007/s00253-022-12296-0